Antisloshing Trajectories for High-Acceleration Motions in Automatic Machines

Anti-sloshing trajectories for high-acceleration motions in automatic machines

Luca Guagliumi
PhD student,
Department of Industrial Engineering
University of Bologna
Bologna, Italy 40137
Email: luca.guagliumi3@unibo.it

Alessandro Berti
R&D departement Marchesini Group S.p.a.
Pianoro (BO), Italy 40065
Email: alessandro.berti@marchesini.com

Eros Monti
R&D departement Marchesini Group S.p.a.
Pianoro (BO), Italy 40065
Email: eros.monti@marchesini.com

Marco Carricato
Full Professor,
Department of Industrial Engineering
University of Bologna
Bologna, Italy 40137
Email: marco.carricato@unibo.it

This paper studies the design of anti-sloshing trajectories for application in automatic machines for packaging liquid products, with specific reference to cylindrical containers and emphasis on prescribed motion durations. Different strategies, based on a discrete linear model of the sloshing phenomenon and applicable in real-time, are analyzed to perform anti-sloshing feedforward control of the container motion: FIR filters (input shapers and others), dynamic-model inversion, and IIR filters. Unlike the previous literature, these strategies are applied to highly dynamical motion laws, with maximum accelerations from $4m/s^2$ *to* $13m/s^2$*. The effectiveness of the proposed anti-sloshing trajectories is assessed by experiments.*

Keywords — Sloshing, Anti-sloshing trajectories, Input shaping, IIR filters, FIR filters, Experimental Analysis.

1 Introduction

When a container partially filled with a liquid is moved, the *sloshing* phenomenon arises, i.e., the uncontrolled vibration of the liquid free surface. The high productivity required by automatic machines for packaging liquid products leads to the necessity of using highly dynamic trajectories to move the products, with accelerations and velocities roughly up to $10m/s^2$ and $2m/s$, respectively. Due to these demanding motion laws, the liquid free-surface oscillation may cause the product to overflow, which is an undesired effect. Even when no liquid spilling occurs, it is often required to dirty the container walls as little as possible. Accordingly, the trajectory designer must choose the most suitable motion law to maintain the liquid motion under control, in spite of the stringent productivity requirements.

The problem of designing an optimal anti-sloshing motion law is well known in the literature. In [1] a sliding-mode controller is designed, which is based on the ability to measure the sloshing height and its rate of change in real-time; however, these measurements are difficult to obtain. A study specifically related to the packaging industry is presented in [2] and [3], with the objective of finding a reference trajectory to limit the liquid sloshing in rectangular containers. Reference [2] develops a minimum-energy-based optimization problem, whereas Ref. [3] uses an iterative learning

control, based on measurements of the liquid state collected in an experimental testbed: both approaches are numerical and computationally intensive. Another approach based on a constraint optimization problem is studied in [4] for building time-optimal spatial trajectories. In [5] a hybrid-shape approach using notch and low-pass filters is proposed for 3-D spatial paths, while in [6], a similar method based on a time-varying notch filter is applied with an interesting use of the container tilting; indeed, an appropriate change in the container orientation can be used to reduce sloshing also in complex spatial movements [7]. However, the tilting-based approach cannot be used if the container orientation must remain constant, as is often the case in packaging lines.

Another class of approaches to design anti-sloshing trajectories is based on optimization techniques for linear dynamic systems. The Input Shaping is a method based on a particular class of Finite Impulse Response (FIR) filters. It is used to reduce sloshing in a cylindrical container moved by a robotic manipulator along rectilinear paths in [8]and along more complex spatial motions in [9]. A general study about robust shapers is presented in [10] and validated by experimentation on a rectangular container. In [11] an input shaper is combined with command smoothing to suppress sloshing not only for the first oscillation mode, but also for higher ones. Input shaping is also applied to more complex situations: for example, in [12], the flexibility of the conveyor belt used for the container motion is considered in the model, and in [13] the container is suspended like a pendulum. The latter situation is analyzed in several recent studies, since it represents the practical application of cranes moving filled containers (as in the casting industry), where command shaping procedures similar to input shaping are used to suppress the liquid free surface vibration: a sequence of steps is used in [14], a multisine-wave function is used in [15] and a smooth polynomial shaped command is proposed in [16]. Another method based on the same assumptions as input shaping is applied in [17] to a linearized model describing sloshing in a rectangular container. Though input shaping is the most common strategy, the literature also presents other solutions to generate anti-sloshing trajectories for linear dynamic systems based on different FIR exponential filters [18] or Infinite Impulse Response (IIR) filters [19]. All these methods share the drawback of introducing a delay in the system response. Moreover, to our knowledge, all techniques based on a linear dynamic model are analyzed and validated in the literature only for motions with relatively low dynamics, with maximum accelerations of the container in the order of $2.5 m/s^2$ or lower. However, in automatic packaging machines, container trajectories must have a specified duration to allow synchronized operations performed on the product, and the involved accelerations achieve much higher values.

In a previous work [20], we developed a simple and general method to predict the sloshing height when the container moves on a prescribed planar path. The technique was then studied also on more complex spatial movements performed by an industrial robot [21]. This method uses the *linear mass-spring-damper model* for sloshing. We showed by experimental tests that this technique is suitable to estimate the maximum sloshing height reached by the free surface even for highly dynamic container motions, with maximum acceleration up to $12 m/s^2$. This suggests us to study if the linear mass-spring-damper model and the vibration-mitigation techniques valid for linear dynamic systems can be used to design anti-sloshing trajectories even when high container accelerations are involved. Accordingly, the current paper has the following objectives:

1. to evaluate the applicability of anti-sloshing optimization methods for linear dynamic systems in highly dynamic motions with container accelerations higher than $2.5 \div 3 m/s^2$, for which the assumptions at the basis of the linear mass-spring-damper model are not obviously satisfied;
2. to compare, by employing experimental tests, the aforementioned optimization methods to obtain anti-sloshing trajectories;
3. to give practical tips to generate anti-sloshing motion laws with a prescribed duration, paying particular attention to real-time applicability.

We will focus on fast rest-to-rest rectilinear motions, and we will aim at both controlling the maximum sloshing height during movement and the residual oscillation of the liquid after the motion ends. Indeed, intermittent rectilinear motions are the most common in automatic packaging machines, so that after each movement there is a rest period before the successive translation. Accordingly, on the one hand, the maximum sloshing height during motion must be kept below a given threshold to prevent the liquid from overflowing or dirtying the container walls. On the other hand, residual oscillations after the motion end must be quickly suppressed since they would add to the ones generated by the subsequent translation, thus exponentially increasing.

Finally, we will consider cylindrical containers partially filled with water since this shape is the most common in automatic packaging machines and low-viscosity liquids (like water) are those for which sloshing effects are more significant.

The paper structure is as follows. Section 2 briefly presents the discrete linear model used to describe sloshing. Section 3 presents several optimization methods to obtain anti-sloshing trajectories based on the linear model. Section 4 studies the design of motion laws with a prescribed duration. Section 5 analyzes the problem of using trajectories with high accelerations. Section 6 shows the results of the experimental tests. Finally, conclusions are drawn in Section 7.

2 Sloshing model

A complete analytical study about sloshing is presented in [22]. Therein, a continuum model is studied under the assumptions of an incompressible, irrotational, and non-viscous fluid. For applications in the gravitational field, capillarity and surface tensions can be neglected. From the continuum model and for a cylindrical container, one can compute the generic natural frequency of the m-th circumferen-

tial mode and the n-th radial mode as:

$$\omega_{mn} = \sqrt{\frac{g\xi_{mn}}{R} tanh\left(\frac{\xi_{mn}h}{R}\right)} \quad (1)$$

where R is the internal radius of the container, h is the filling height in static conditions, g is the gravity acceleration, and ξ_{mn} is one of the roots of the Bessel function derivative with respect to the radial coordinate r (its values are known constants tabulated in [23]). Only the fundamental circumferential mode can be considered ($m = 1$) since the other ones are negligible [22], so that, for the sake of conciseness, we can set $\omega_{1n} = \omega_n$ and $\xi_{1n} = \xi_n$.

Different equivalent discrete models can be derived by imposing the same mass properties, oscillation modes, and inertia wrenches exerted on the container walls as in the continuum model. A discrete mass (*sloshing mass*) represents every mode of the continuum model. One or more differential equation describe the motion of each sloshing mass. The complexity of the discrete models grows with the complexity of the free-surface movement that we want to represent: if we want to describe the non-linear behavior of the liquid, also the motion equations of the sloshing masses should be non-linear, and if we want to describe *rotary sloshing* [22], we need two (coupled) motion equations for one sloshing mass. Springs (or pendulums) and dampers connect every sloshing mass to the container walls. The higher is the number of used masses, the higher is the model precision. For each discrete mass, the damping coefficient is estimated by empirical formulations; for a cylindrical container filled with a fluid with density ρ and dynamic viscosity μ, we can use [22]:

$$\zeta_n = 0.92\sqrt{\frac{\mu/\rho}{\sqrt{gR^3}}} \cdot \left[1 + \frac{0.318}{sinh\,(1.84h/R)}\left(1 + \frac{1-h/R}{cosh\,(1.84h/R)}\right)\right] \quad (2)$$

The discrete linear model is presented in [22] and his schematic representation is shown in Fig. 1, where the liquid free surface is assumed to remain planar during its oscillations. Every sloshing mass m_n is connected to a stiffness k_n and to a damper with damping constant $c_n = 2\zeta_n\omega_n m_n$. The natural frequency of the nth mass is equal to the one of the nth sloshing mode, i.e. $\omega_n = \sqrt{(k_n/m_n)}$. A fixed mass m_0 represents the liquid that does not take part in the sloshing phenomenon. The nth sloshing mass motion equation is:

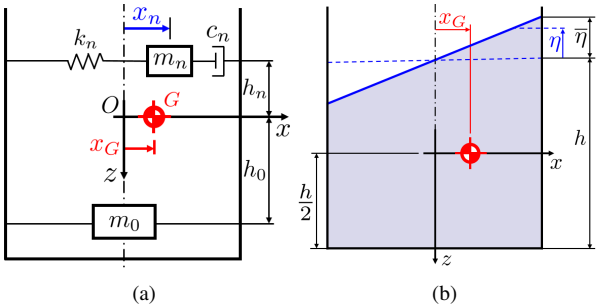

Fig. 1: Linear mass-spring-damper model (a) and representation of the liquid free surface (b).

$$\ddot{x}_n + 2\zeta_n\omega_n\dot{x}_n + \omega_n^2 x_n = -\ddot{x}_0 \quad (3)$$

where $\ddot{x}_0$ is the container acceleration.

By integrating Eq. (3) for every n, one can compute the evolution in time of x_n for every container motion law. According to [20], the maximum sloshing height at the container wall can be estimated as:

$$\overline{\eta} = 8\sum_n \frac{x_n}{\xi_n(\xi_n^2 - 1)} tanh\left(\xi_n\frac{h}{R}\right) \quad (4)$$

3 Optimization based on the linear model

This Section analyzes a class of methods based on the linear model described in Section 2 to design trajectories that mitigate liquid sloshing in the container. These methods are applied to some of the most common trajectories used in automatic packaging machines, such as polynomial (like poly5) and modified trapezoid acceleration trajectories [24]. The latter are obtained by connecting constant acceleration segments with sinusoidal functions (eg. Traj. 1 in Fig. 9(a)).

For the application of all the anti-sloshing techniques described in this Section, only the fundamental mode of the model is considered (the one described by Eq. (3) with $n = 1$), for a reason that will be clarified at the end of Section 4.

3.1 Input shaping

Input shaping for linear dynamic systems is a well-known technique [25]. The main idea consists in performing a convolution between a train of impulses (the input shaper) and a motion law, and then applying the resulting trajectory to the system. The amplitude and the time delay of the impulses can be calculated to cancel the residual oscillation of the response. The amplitude of the residual vibration related to the nth mode of a mechanical system subjected to a train of $N+1$ impulses is:

$$Z_n(\omega_n, \zeta_n) = \sqrt{\left[\sum_{j=0}^{N} B_j\, cos\,(\gamma_j)\right]^2 + \left[\sum_{j=0}^{N} B_j\, sin\,(\gamma_j)\right]^2}$$

with:

$$\gamma_j = \omega_n\sqrt{1-\zeta_n^2}\,(t_N - t_j) \quad , \quad B_j = \frac{A_j\omega_n e^{-\zeta_n\omega_n(t_N - t_j)}}{\sqrt{1-\zeta_n^2}}$$

where A_j is the amplitude of the jth impulse and t_j is its time delay.

To obtain a zero vibration (ZV) shaper (by a train with two impulses, i.e. $N = 1$) the following conditions must be imposed:

1. the amplitude of the residual vibration at the end of the train of impulses is equal to zero: $Z_n(\omega_n, \zeta_n) = 0$;
2. the first impulse has no delay: $t_0 = 0$;
3. the train of impulses is normalized so that the steady-state response of the shaped law is equal to the original one: $\sum_{j=0}^{N} A_j = 1$.

Similarly, we can calculate the parameters for robust shapers by imposing to cancel the amplitude of the residual vibration and its derivatives with respect to the natural frequency. With three and four impulses, we obtain, respectively, a zero vibration derivative (ZVD) shaper and a zero vibration derivative - derivative (ZVDD) shaper. This procedure is useful when the system's parameters (in particular its natural frequency) are not sure, which is very common in practice. By imposing these conditions, we can compute the parameters of every shaper, which depend on:

$$K = e^{-\zeta_n \pi / \sqrt{1-\zeta_n^2}} \quad , \quad T = \frac{2\pi}{\omega_n \sqrt{1-\zeta_n^2}} \tag{5}$$

In particular, if v is the highest derivative order of Z_n that is set to zero, $v+2$ impulses must be used, each one with a time delay equal to:

$$t_j = \frac{T}{2} j \quad , \quad j = 0, 1, \ldots, v+1 \tag{6}$$

The amplitudes A_j of the impulses are functions of the parameter K in Eq. (5), and their values are different for different shapers [25].

A robust shaper may also be built by admitting a certain percentage of residual vibration $\bar{z}$, thus obtaining a so-called extra-insensitive (EI) shaper. In particular, for the one-hump shaper, we have three impulses with time delays expressed by Eq. (6) and amplitudes that are functions of $\bar{z}$ [26]. We can also use EI shapers with more humps to achieve a more robust behavior.

The use of any input shaper always causes a delay in the system response, which is equal to the time delay of the last impulse, and so it is given by Eq. (6), with $j = v+1$. Thus, the main drawback of robust shapers is that the more robust the method, the higher the introduced delay.

3.2 Inversion of the dynamic model

The general idea at the basis of the inversion of the dynamic model is to filter the input trajectory with an appropriate transfer function that yields a response like the one of a first-order dynamic system [24]. In the following, a specific declination for the sloshing problem at hand is provided.

For the linear mass-spring-damper model, the transfer function between the container trajectory $x_0(t)$ and the displacement of the sloshing mass with respect to a fixed reference frame, namely $x_{nAbs}(t) = x_n(t) + x_0(t)$, is:

$$G_1(s) = \frac{k_n + c_n s}{m_n s^2 + c_n s + k_n} = \frac{\omega_n^2 + 2\zeta_n \omega_n s}{s^2 + 2\zeta_n \omega_n s + \omega_n^2}$$

where s is the variable of the Laplace domain. We can modify the motion law $x_0(t)$ by pre-multiplying it by a transfer function $F_{inv}(s)$ such that $F_{inv}(s) \cdot G_1(s) = 1$, namely $F_{inv}(s) = 1/G_1(s)$, thus obtaining a new trajectory $y_0(t)$:

$$y_0(t) = \mathcal{L}^{-1}\{F_{inv}(s)\mathcal{L}\{x_0(t)\}\} \tag{7}$$

where the operators $\mathcal{L}\{-\}$ and $\mathcal{L}^{-1}\{-\}$ represent respectively the Laplace transform and the inverse Laplace transform of a given function. Clearly, this way, $x_{nAbs}(t) = x_0(t)$ and so: $x_n(t) = x_0(t) - y_0(t)$. From here,

$$\mathcal{L}\{x_n(t)\} = -\frac{1}{\omega_n^2} \cdot \frac{1}{1 + (2\zeta_n/\omega_n)s} \mathcal{L}\{\ddot{x}_0(t)\}$$

This is exactly the response of a first-order dynamic system with a time constant equal to $2\zeta_n/\omega_n$. This value is always near to zero, because $\zeta_n \approx 0$ and $\omega_n > 1$. This means that the delay introduced in the response is, in practice, negligible. This is useful because we want to design trajectories with a prescribed duration. However, this method requires a good knowledge of the dynamic-model parameters to be effective, and this causes a noticeable lack of robustness.

3.3 Infinite Impulse Response (IIR) filters

Infinite Impulse Response (IIR) filters were proposed in [27] to reduce the uncontrolled oscillations of flexible mechanical systems. They were later applied in [19] to damp the oscillations of a liquid in a container. The idea is similar to the inversion of the dynamic model, but now the filter is designed to produce a response on the mass-spring-damper like the one of a critically damped second (or third) order system. In practice, we are looking for a transfer function $F_{IIR}(s)$ such that $G_{d2}(s) = F_{IIR}(s)G(s)$, with $G(s)$ being the transfer function of the linear model (3) and $G_{d2}(s)$ being:

$$G_{d2}(s) = -\frac{1}{\omega_n^2} \frac{\tau^2}{(s+\tau)^2}$$

Accordingly:

$$F_{IIR}(s) = \frac{1}{\omega_n^2} \frac{\tau^2}{(s+\tau)^2} \left(s^2 + 2\zeta_n \omega_n s + \omega_n^2\right) \tag{8}$$

Here, τ is a parameter chosen to manage the delay introduced in the response. If τ is high, the delay is small. In particular, if $\tau \to +\infty$, we obtain the same result achieved by the inversion of the dynamic model.

A filter like (8) can produce an initial unwanted peak in the response. To avoid it, we may opt for a critically-damped system of the third order:

$$G_{d3}(s) = -\frac{1}{\omega_n^2}\frac{\tau^3}{(s+\tau)^3}$$

so that:

$$F_{IIR}(s) = \frac{1}{\omega_n^2}\frac{\tau^3}{(s+\tau)^3}\left(s^2+2\zeta_n\omega_n s+\omega_n^2\right) \tag{9}$$

To calculate the optimized container trajectory $\ddot{y}_0$, we have to apply the Laplace transform to the original motion law $\ddot{x}_0$, then multiply the result by the transfer function $F_{IIR}(s)$, and finally apply the inverse Laplace transform. This procedure is computationally expensive. Alternatively, by using the Z-transform ($\mathcal{Z}\{-\}$) on $F_{IIR}(s)$, we can obtain a finite difference equation that allows us to find the output of the filter in sampled instants of time. Procedures to do so are described in [27] and [19], but they give results with a low precision for a sampling period of $1ms$, which is common in industrial applications. An alternative method, based on the theory of digital control [28], is proposed hereafter. The idea is to use a First-Order Hold (FOH) so that the discrete formulation equivalent to a general transfer function $H(s)$ is:

$$H(z) = \frac{z-1}{T_s z}\mathcal{Z}\left\{\frac{H(s)}{s^2}\right\} \tag{10}$$

where T_s is the sampling period. By applying the transformation (10) to Eq. (8), if $y(k)$ is the output filtered trajectory and $u(k)$ is the input trajectory at the sampled instant k, then:

$$\begin{aligned} y(k) = &-a_1 y(k-1) - a_2 y(k-2) + \\ &+ b_0 u(k+1) + b_1 u(k) + b_2 u(k-1) + b_3 u(k-2) \end{aligned} \tag{11}$$

where:

$$\begin{aligned} &a_1 = -2e^{-\tau T_s} \;\;,\;\; a_2 = e^{-2\tau T_s} \;\;,\;\; b_0 = Q(A+C) \\ &b_1 = Q\left[(-2A-C+DT_s)e^{-\tau T_s} - A + BT_s - 2C\right] \\ &b_2 = Q\left[Ae^{-2\tau T_s} + (2A-2BT_s+2C-2DT_s)e^{-\tau T_s} + C\right] \\ &b_3 = Q\left[(-A+BT_s)e^{-2\tau T_s} + (-C+DT_s)e^{-\tau T_s}\right] \end{aligned}$$

and the constants are:

$$\begin{aligned} &Q = \left(\frac{\tau}{\omega_n}\right)^2\frac{1}{T_s} \;\;,\;\; A = \frac{2\left(\zeta_n\omega_n\tau-\omega_n^2\right)}{\tau^3} \;\;,\;\; B = \left(\frac{\omega_n}{\tau}\right)^2 \\ &C = \frac{-2\left(\zeta_n\omega_n\tau-\omega_n^2\right)}{\tau^3} \;\;,\;\; D = \frac{\tau^2-2\zeta_n\omega_n\tau+\omega_n^2}{\tau^2} \end{aligned}$$

In the same way, by applying transformation (10) to Eq. (9), we find:

$$\begin{aligned} y(k) = &-a_1 y(k-1) - a_2 y(k-2) - a_3 y(k-3) + \\ &+ b_0 u(k+1) + b_1 u(k) + b_2 u(k-1) + \\ &+ b_3 u(k-2) + b_4 u(k-3) \end{aligned} \tag{12}$$

where:

$$\begin{aligned} &a_1 = -3e^{-\tau T_s} \;\;,\;\; a_2 = 3e^{-2\tau T_s} \;\;,\;\; a_3 = -e^{-3\tau T_s} \\ &b_0 = Q(A+C) \\ &b_1 = Q\left[(-3A-2C)e^{-\tau T_s} - A - 2C + \overline{D} + \overline{E} + BT_s\right] \\ &b_2 = Q\left[(3A+C)e^{-2\tau T_s} + \right. \\ &\quad \left. + \left(3A-3BT_s+4C-\overline{D}+\overline{E}\right)e^{-\tau T_s} + C - 2\overline{D} - 2\overline{E}\right] \\ &b_3 = Q\left[-Ae^{-3\tau T_s} + (-3A+3BT_s-2C)e^{-2\tau T_s} + \right. \\ &\quad \left. + \left(-2C+2\overline{D}-2\overline{E}\right)e^{-\tau T_s} + \overline{D} + \overline{E}\right] \\ &b_4 = Q\left[(A-BT_s)e^{-3\tau T_s} + Ce^{-2\tau T_s} + \left(-\overline{D}+\overline{E}\right)e^{-\tau T_s}\right] \end{aligned}$$

and:

$$\begin{aligned} &Q = \frac{\tau^3}{\omega_n^2}\frac{1}{T_s} \;\;,\;\; A = \frac{2\zeta_n\omega_n\tau-3\omega_n^2}{\tau^4} \;\;,\;\; B = \frac{\omega_n^2}{\tau^3} \\ &C = \frac{-2\zeta_n\omega_n\tau+3\omega_n^2}{\tau^4} \;\;,\;\; D = \frac{-2\left(\zeta_n\omega_n\tau-\omega_n^2\right)}{\tau^3} \\ &\overline{D} = DT_s e^{-\tau T_s} \;\;,\;\; E = \frac{\tau^2-2\zeta_n\omega_n\tau+\omega_n^2}{\tau^2} \;\;,\;\; \overline{E} = E\frac{T_s^2}{2}e^{-\tau T_s} \end{aligned}$$

In both Eq. (11) and Eq. (12), we notice the presence of the term $u(k+1)$. This means that the output motion law in the instant k also depends on the value of the input trajectory in the next instant $k+1$. In fact, using a FOH leads to a non-casual filter (i.e., the output after filtering also depends on future values of the input). In some applications, non-causality cannot be tolerated, but in our case, it is acceptable since the original trajectory is completely known at every instant, and so we can easily evaluate the term $u(k+1)$.

3.4 Multi-segment trajectories based on Finite Impulse Response (FIR) filters

Reference [29] proposes a new method to design multi-segment trajectories with time and frequency constraints. The idea is to use a sequence of Finite Impulse Response (FIR) filters to filter an input step with an amplitude equal to the length of the motion required. Every filter of the chain represents a rectangular window function with duration T_i and amplitude $1/T_i$ (i.e., the window area is 1). In the Laplace domain, the generic FIR filter is represented by:

$$M_i(s) = \frac{1}{T_i}\frac{1-e^{-sT_i}}{s} \tag{13}$$

With a chain of three FIR filters like the one in Eq. (13) we obtain a trajectory with a trapezoid acceleration, which is

common in automatic packaging machines. Reference [29] suggests to calculate T_1 and T_2 by a method based on the maximum velocity and acceleration allowed by the application at hand. However, for the aim of this paper, the choice of T_3 is more important. In fact, by suitably choosing T_3, we can find a motion law that cancels the residual vibration of the system. To achieve this aim, Ref. [30] suggests to approximately calculate T_3 (for a damped system) as in Eq. (5).

Once T_1, T_2, and T_3 are chosen, we can calculate the final motion law by right-multiplying the original step transform by the transfer functions of the filters, and then applying the inverse Laplace transform. It is interesting to notice that, if the following conditions are satisfied, the obtained trajectory has a trapezoid acceleration profile:

$$\begin{cases} T_1 \geq T_2 + T_3 \\ T_2 \geq T_3 \end{cases} \tag{14}$$

For damped systems, instead of using a classical FIR filter, expressed in the Laplace domain by (13), Ref. [30] suggests the use of an exponential FIR filter. This filter is more complex and also gives a more complex trajectory. We did not use it in this paper because, for low-viscosity liquids like the ones used in our application, it provides motion laws very similar to those obtained with the classical FIR filter, which is simpler to use.

Like for the trajectories obtained with an IIR filter, calculating the output motion law using the inverse Laplace transform is computationally expensive. For this reason, here too, we can apply the Z-transform to find a finite difference equation to obtain the output of each FIR filter of the chain. Reference [29] suggests an expression based on the integration backward-difference formula, but this approach is not accurate for a sampling period of $1ms$. A more precise formula can be obtained based on numerical integration by the trapezoid rule:

$$q_i(k) = q_i(k-1) + \frac{1}{2N_s}\left[q_{i-1}(k) + q_{i-1}(k-1) + \right. \\ \left. - q_{i-1}(k-N_s) - q_{i-1}(k-N_s-1)\right] \tag{15}$$

Here, N_s is the number of samples, and $q_i(k)$ and $q_{i-1}(k)$ are, respectively, the output and input trajectories to the ith filter of the chain at the sampled instant k. For the first filter, the input is a step function with amplitude equal to the total movement described by the final trajectory.

4 Computation of trajectories with a prescribed motion duration

We have already mentioned that it is important to design trajectories with a prescribed time in the field of automatic packaging machines. In contrast, many optimization techniques presented in Section 3 introduce time delays.

The delay ΔT introduced by an input shaper is known in advance. For example, with a ZV shaper, setting $j = 1$ in Eq. (6), $\Delta T = T/2$, where T is expressed by (5) and it can be computed by means of the model parameters. For a ZVD shaper, ΔT is doubled, and so on. If we want a trajectory with a total time equal to t_f, it suffices to apply a shaper to a trajectory with a total duration equal to $t_f - \Delta T$, as done in [31]. The value of ΔT is distinct for different shapers, but Eqs. (5) and (6) allow to easily calculate it. The drawback of this procedure for practical applications is that the container acceleration and/or jerk may reach high values: in general, the more so with increasing values of ΔT (see the motion laws in Figures 7(a) and 8(a) as examples).

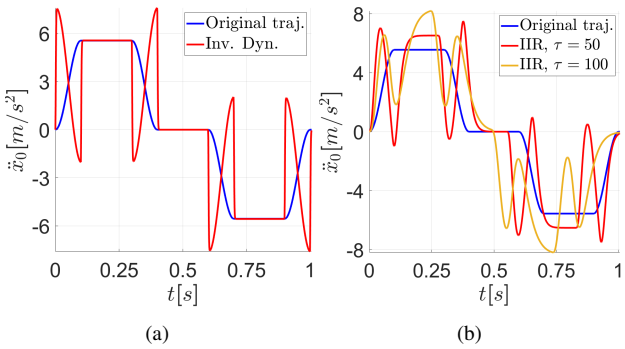

(a) (b)

Fig. 2: Trajectories obtained by applying the inversion of the dynamic model (a) and the IIR filtering (b) to a modified trapezoid acceleration motion on the large container described in Section 6.

The dynamic model inversion produces a trajectory with a delay that is practically zero. However, this technique has other problems. The first one is the already-mentioned lack of robustness (see Section 3.2). The second problem is that there is no control on the trajectory obtained after applying the method. For example, suppose we use a modified trapezoid acceleration profile with a total duration equal to $1s$. In that case, we get an optimized motion law like the one in Fig. 2(a) for the large container described in Section 6. Such an acceleration profile has a trend with too many oscillations and jumps, which is harmful in practice: it can trigger vibrations of mechanical components, resulting in a negative effect on the liquid sloshing. For these reasons, the method of dynamic-model inversion was discarded.

Like input shaping, IIR filters introduce a delay in the system response, but in this case, we do not know a priori the amplitude of the delay because it depends on both the constant τ in Eqs. (8) and (9) and the input trajectory. After setting a value for τ, we can compute and simulate the filtered trajectory, thus evaluating the introduced delay ΔT. Then, we can calculate a new motion law with a total time equal to $t_f - \Delta T$, and so we can apply the IIR filter again to this new trajectory. We can reiterate the procedure until the difference between the duration of the filtered trajectory and t_f is less than $1ms$. In practice, one iteration is usually sufficient. As far as the choice of parameter τ is concerned, if τ is too large, the delay introduced is too small, and the filter gives results similar to those provided by the dynamic-model inversion with the corresponding drawbacks. If τ is too small,

the delay introduced is too high: the new trajectory has a total duration $t_f - \Delta T$ too short, and the acceleration peaks can be too high. The choice of τ is thus a trade-off between these two aspects. For motion laws like the ones analyzed in this paper (with a total time of about $1s$) and for cylindrical containers, a value of τ between 40 and 100 was heuristically found to be in most cases adequate. We also notice that the acceleration profile obtained by the application of an IIR filter to a modified trapezoid acceleration trajectory for the large container, in Fig. 2(b), has too many oscillations, and so it is not suitable for a real application. For this reason, in the experimental tests, IIR filters are applied only on poly5 trajectories for the large container. At the same time, they are used on modified trapezoid acceleration motion laws for the medium vessel.

The use of FIR filters as described in Section 3.4, directly produce a motion law with a known duration determined by the number of filters that are used. By considering a sequence of three filters, the total duration of the optimized motion law is equal to $T_1 + T_2 + T_3$. We have seen in Section 3.4 that the parameter T_3 can be computed by Eq. (5), and so it only depends on the characteristics of the system. This means that the parameters T_1 and T_2 must be chosen such that $T_1 + T_2 = t_f - T_3$ and so, to satisfy this relation, only one of these parameters can be freely chosen. It is interesting to notice that conditions (14) may not always be satisfied. If this happens, the resulting acceleration profile is not trapezoidal. However, the motion law is still simple (see Opt. Traj. 15 in Fig. 9(a)) and able to cancel the residual vibrations of the system. The use of FIR filters to design anti-sloshing trajectories with a prescribed duration is very interesting because, unlike the other methods, it provides motion laws with a simple shape and so easy to apply in practical cases. This is also the main difference with the results reported in Ref. [18], where exponential FIR filters were used to obtain more complex anti-sloshing trajectories, inducing time delays in the response.

It is possible to apply all anti-sloshing methods not only to the fundamental mode, but also to the higher ones. For example, this is done in [32] with input shaping. However, this strategy is not applied in this paper, since every mode taken into account produces a higher delay in the movement. This means that if we want to damp more than one mode of the liquid free surface, it is necessary to use shorter motion laws, and the benefit obtained by smoothing higher-mode vibrations is canceled out by the higher accelerations reached by the container.

5 High-acceleration effects

This Section analyze the problem of using trajectories characterized by high accelerations.

First of all, high values of container acceleration produce high amplitude oscillations of the liquid free surface. One of the main assumptions for building the discrete linear model for the sloshing described in Section 2 is to consider small oscillations of the free surface. For high accelerations of the container, this is not strictly true. However, the anti-

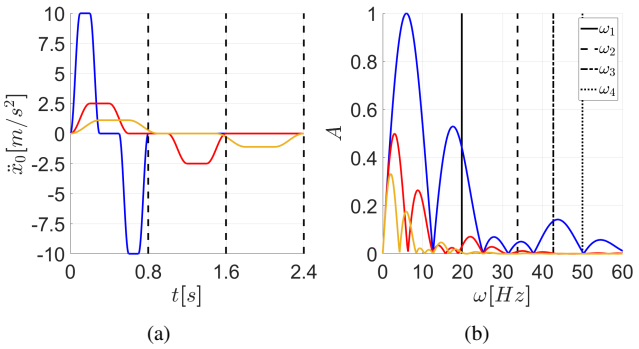

(a) (b)

Fig. 3: Three modified trapezoid motion laws with different maximum accelerations (a) and their harmonic content (b).

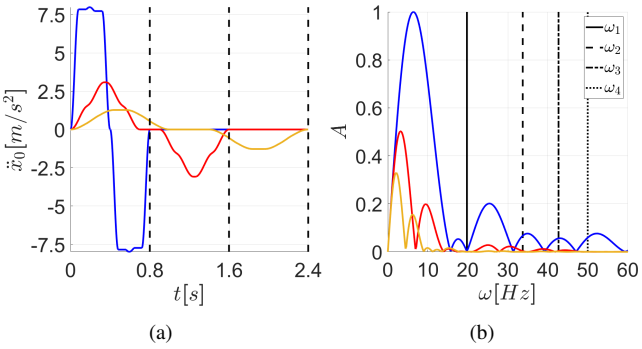

(a) (b)

Fig. 4: Trajectories shown in Fig 3(a) modified with a ZV shaper (a) and their harmonic content (b).

sloshing methods presented in Section 3 are based on the linear model, so it is interesting to verify whether they are still valid when the conditions to build the model are not necessarily respected.

The second problem is related to the harmonic content of high-acceleration motion laws. We can consider the motion laws in Figs. 3 and 4 as an example. In Fig. 3(a) three different modified trapezoid acceleration motion laws are shown. All trajectories perform a one-meter movement and they have the same shape, but their duration is different ($0.8s$, $1.6s$ and $2.4s$). This produces maximum accelerations that are higher for shorter motion laws. The harmonic content of the trajectories, obtained by the Fourier transform, is shown in Fig. 3(b), normalized with respect to the maximum value. We can notice that the higher the container acceleration, the higher the amplitude spectrum of the motion law. In particular, the harmonic content of the trajectories in correspondence to the natural frequencies $\omega_1, \omega_2, \omega_3, \omega_4$, of the free surface is important: when accelerations are high, it is easier to have high peaks corresponding to the first sloshing mode and also to excite higher modes. When we apply an anti-sloshing method (for example, in Fig. 4(a), the trajectories shown in Fig. 3(a) are modified with a ZV shaper), the harmonic content of the motion law is modified by cutting the frequencies that correspond to the first mode (4(b)). However, when high accelerations are reached, the higher

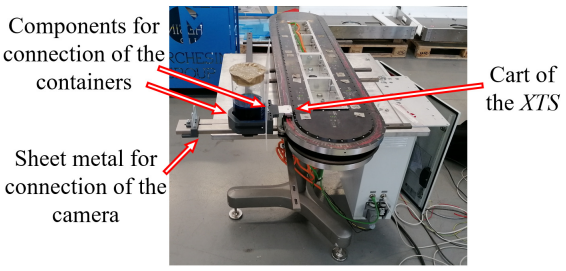

(a)

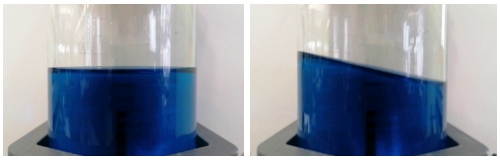

(b) (c)

Fig. 5: Experimental setup (a) and frames taken from recorded videos when the container is at rest (b) or in motion (c).

modes are still excited and, even if their contribution is lower, they still cooperate to generate sloshing.

Moreover, we can notice that the harmonic content of the low acceleration motion laws is much flatter than the the content of the high-acceleration trajectory near the fundamental mode. This means that even if the estimated natural frequency in Eq. (1) differs from the real one, the anti-sloshing method proves effective, whereas a little difference in the real natural frequency for the high-acceleration motion law has a greater influence on the liquid behavior.

6 Experimental results

This Section reports the experimental tests performed to verify the effectiveness of the methods described in Sections 3 and 4 to design anti-sloshing trajectories. Figure 5(a) shows the test bench: a *Beckhoff XTS* with a $1m$-long rectilinear stroke is used to perform different trajectories, and a camera mounted on the *XTS* cart is used to record videos of the liquid free surface; from the analysis of the frames (like the ones in Fig. 5) the evolution in time of the sloshing height is derived. Cylindrical containers with different diameters ($27mm$, $50mm$, $92mm$) were tested. The volume of water in the small, medium, and large container is respectively $15170mm^3$, $80500mm^3$, and $500000mm^3$. A minimal amount of blue dye was introduced into the water to ease the observation of the liquid motion. The quantity of dye was so small to change the fluid properties (density, viscosity, and surface tension) in no appreciable way. Due to the reduced diameter of the small container ($27mm$), the liquid sloshing in experimental tests involving this vessel was very small, since a small diameter tends to reduce the vibrations of the free surface, even when anti-sloshing motion laws are not used. This is probably caused by the effect of the surface tension of the liquid, which becomes more important in the modeling of the system when small diameters are involved. However, in this study, we are interested in showing the effectiveness of anti-sloshing methods for movements with high accelerations. Thus, the interest in applying these techniques to systems that are already well-damped is minimal. For this reason, only the results regarding the medium and large containers are discussed in the following.

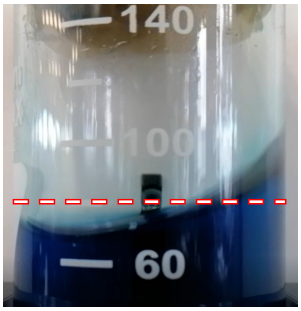

Fig. 6: Liquid surface shape during the free response of the system after the container motion ends. The dashed line represents the liquid level at rest.

In the experimental results (Figures 7-13) we often notice an asymmetrical behavior of the liquid free-response, after the container motion ends. The positive and negative amplitudes of the free surface oscillation are not centered with respect to the rest plane, because its shape is not planar as assumed by the linear model. We can see an example in Fig. 6. This is probably due to the non-linear behavior of the system that is caused by large oscillations and rotary sloshing.

6.1 Motion laws with a prescribed duration

All the methods described in Section 3, except the dynamic model inversion, were applied to several motion laws with prescribed duration, performing a $1m$ movement in $1s$ for the large container and $0.8s$ for the medium container, thus achieving high accelerations, roughly from 6 to $13m/s^2$. Data about the motion laws and the corresponding responses are listed in Tables 1 and 2, respectively for the large and the medium container. The original motion law and the applied optimization method are listed in the second and the third column. The maximum acceleration and velocity reached during the movement are shown in columns four and five. $\overline{\eta}_{rest}$ is the sloshing height during the rest phase, i.e., at the end of the motion law, when the container is at rest, but the free surface is still oscillating. Then, columns six and seven report the maximum sloshing height measured, respectively, during the container motion and its rest phase. Finally, the last two columns, $\Delta\overline{\eta}_{max}$ and $\Delta\overline{\eta}_{rest}$, report the percentage differences of the maximum sloshing height, respectively during the motion and the rest phase, between the experimental value obtained with the initial trajectory ($\overline{\eta}_{Orig}$) and the optimized one ($\overline{\eta}_{Opt}$):

$$\Delta\eta = \frac{\overline{\eta}_{Opt} - \overline{\eta}_{Orig}}{\overline{\eta}_{Orig}} \cdot 100$$

Table 1: Comparison of the maximum sloshing heights obtained for non-optimized and optimized trajectories of the large container ($t_f = 1s$).

Traj.	Original traj.	Opt. method	$max(\ddot{x}_0)$ $[m/s^2]$	$max(\dot{x}_0)$ $[m/s]$	$max(\overline{\eta})$ $[mm]$	$max(\overline{\eta}_{rest})$ $[mm]$	$\Delta\overline{\eta}_{max}$	$\Delta\overline{\eta}_{rest}$
Traj. 1	Mod. trap.	/	6.2	1.5	60.9	51.8	/	/
Traj. 2	Poly5	/	5.8	1.9	48.9	10.3	/	/
Opt. traj. 8	Mod. trap.	IS-ZV	7.9	1.8	50.4	13.0	−17.2%	−74.9%
Opt. traj. 9	Mod. trap.	IS-EI	6.7	2.1	52.4	24.0	−14.0%	−53.7%
Opt. traj. 10	Mod. trap.	IS-ZVDD	8.5	2.2	48.1	24.2	−21.0%	−53.3%
Opt. traj. 11	Poly5	IS-ZV	6.9	2.8	37.9	13.3	−22.5%	+29.2%
Opt. traj. 12	Poly5	IS-EI	7.3	2.2	40.9	9.5	−16.4%	−7.8%
Opt. traj. 13	Poly5	IS-ZVDD	8.1	2.2	46.4	12.5	−5.1%	+21.4%
Opt. traj. 14	Poly5	IIR ($\tau = 100$)	6.1	1.9	29.3	4.4	−34.8%	−57.3%
Opt. traj. 15	/	FIR	7.9	2.2	39.7	3.5	−34.8%	−93.2%

Table 2: Comparison of the maximum sloshing heights obtained for non-optimized and optimized trajectories of the medium container ($t_f = 0.8s$).

Traj.	Original traj.	Opt. method	$max(\ddot{x}_0)$ $[m/s^2]$	$max(\dot{x}_0)$ $[m/s]$	$max(\overline{\eta})$ $[mm]$	$max(\overline{\eta}_{rest})$ $[mm]$	$\Delta\overline{\eta}_{max}$	$\Delta\overline{\eta}_{rest}$
Traj. 5	Mod. trap.	/	10.0	2.0	47.5	24.6	/	/
Traj. 6	Poly5	/	9.0	2.3	30.9	6.7	/	/
Opt. traj. 16	Mod. trap.	IS-ZV	12.6	2.3	29.8	15.2	−37.3%	−38.2%
Opt. traj. 17	Mod. trap.	IIR ($\tau = 70$)	13.2	2.4	30.2	23.4	−36.4%	−4.9%
Opt. traj. 18	Poly5	IS-ZV	10.8	2.6	26.2	8.6	−15.2%	+28.4%
Opt. traj. 19	Poly5	IIR ($\tau = 70$)	11.3	2.7	31.9	8.9	+3.2%	+32.8%
Opt. traj. 20	/	FIR	11.8	2.7	28.6	15.4	−39.8%	−37.4%

For the FIR filters (which are not used to modify a pre-calculated trajectory, but to build a motion law from scratch), the values are compared with those obtained for the modified trapezoid trajectory.

For the large container, Figures 7 and 8 show the effect of applying different shapers to a modified trapezoid trajectory and a poly5 trajectory, respectively. In the former case (Opt. traj. 8 through 10), the damping effect on the motion law at the end of the movement is significant (the maximum of $\overline{\eta}_{rest}$ is reduced by 75% with Opt. traj. 8). In contrast, for the polynomial trajectory (Opt. traj. 11 through 13), the effect of the shapers is less evident since the initial response is already well-damped. However, a 22.5% reduction in the maximum sloshing height during motion is still obtained with the ZV shaper (Opt. traj. 11). In general, the response to a polynomial trajectory is better than the response

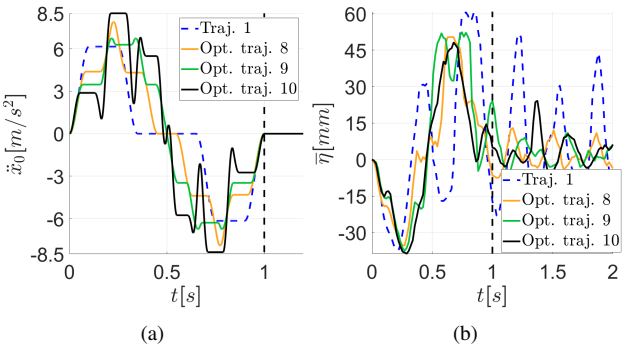

Fig. 7: Acceleration profiles (a) and system responses (b) obtained by the application of different input shapers to a modified trapezoid acceleration trajectory on the large container.

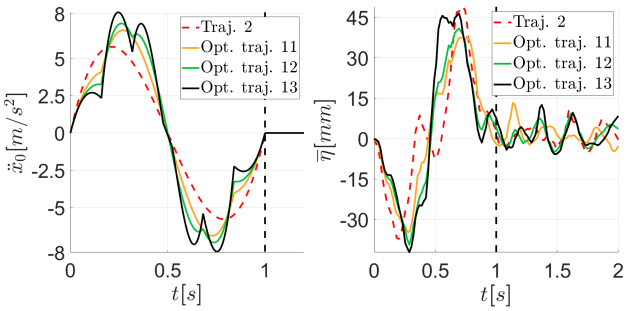

(a) (b)

Fig. 8: Acceleration profiles (a) and system responses (b) obtained by the application of different input shapers to a poly5 trajectory on the large container.

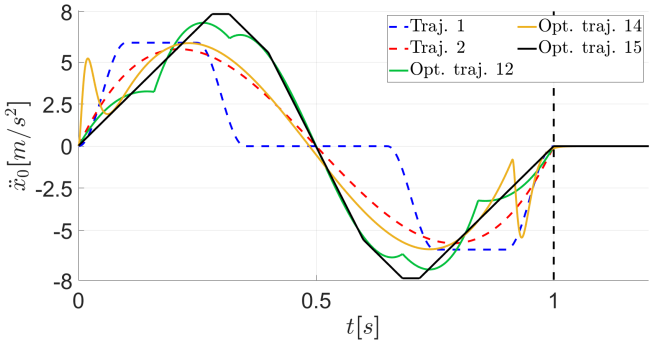

(a)

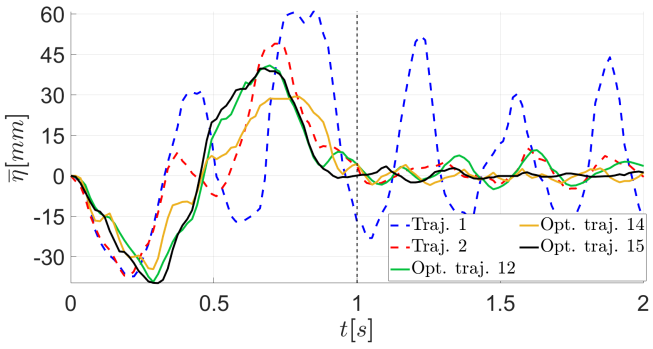

(b)

Fig. 9: Acceleration profiles (a) and system responses (b) obtained by the application of different optimization methods to poly5 and trapezoid acceleration trajectory on the large container.

to a modified trapezoid trajectory, even before optimization. Figure 9 shows a comparison of the system responses obtained by applying different methods, namely EI input shaping (Opt. traj. 12) and IIR filter with $\tau = 100$ (Opt. traj. 14) to a poly5 motion law and a trajectory obtained with a chain of three FIR filters (Opt. traj. 15). The best result is the one received by the application of the IIR filter (Opt. traj. 14), in terms of both maximum sloshing height during the movement and maximum peak of residual vibrations after the motion end, with a reduction of 35% of the former and 57% of the latter compared to the original poly5 law (Traj. 2). If we compare these results with the ones obtained for the modified trapezoid motion law (Traj. 1), the anti-sloshing effect is more marked: the reduction in the sloshing height peak during the container motion increases to 52%, while the one in the rest phase reaches the 92%. These results are not shown in Tables, since they do not measure the effectiveness of the anti-sloshing method itself, but they represent the benefit obtained by a careful choice of the motion law, with the poly5 law generally performing better than the modified trapezoid law. These results show a good effect in reducing the free oscillations of the free surface of the liquid even for motions with very high input accelerations, between $6m/s^2$ and $8.5m/s^2$. Obviously, for the same motion duration, the lower is the maximum acceleration achieved by applying an anti-sloshing method, the better is the result obtained in terms of reduction of maximum sloshing height and residual vibrations of the system.

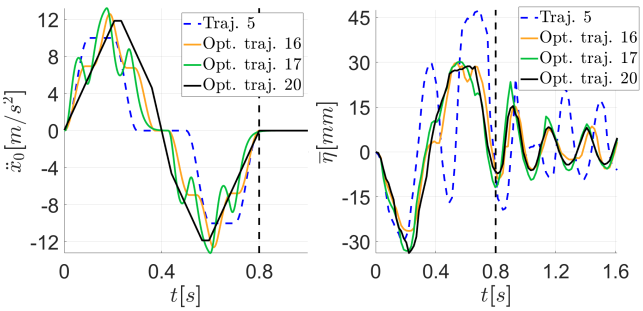

(a) (b)

Fig. 10: Acceleration profiles (a) and system responses (b) obtained by the application of different optimization techniques to a modified trapezoid acceleration trajectory on the medium container.

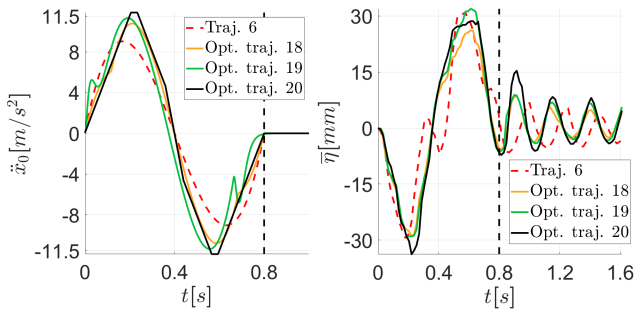

(a) (b)

Fig. 11: Acceleration profiles (a) and system responses (b) obtained by the application of different optimization techniques to a poly5 trajectory on the medium container.

For the medium container, the responses obtained are shown in Fig. 10 and 11. Here, the effectiveness of the anti-sloshing methods is less marked due to the very high accelerations reached (roughly $13m/s^2$). In particular, if we

choose a poly5 trajectory (Traj. 6) for the optimization (Fig. 11), the higher accelerations introduced by the optimization methods (Opt. traj. 18 through 20) produce slightly higher residual vibrations, so there is no apparent benefit in applying anti-sloshing methods. The result is different if we apply the optimization techniques to a worse original trajectory, like a modified trapezoid (Traj. 5 Fig. 10). In this case, the reduction of the maximum sloshing height during the motion and in the rest phase obtained by applying different anti-sloshing methods (Opt. traj. 16, 17, 20) is clear: in both cases, the reduction of the sloshing height may achieve 38%.

6.2 Motion laws without a prescribed duration

Figures 12 and 13 show the results obtained by the classical application of optimization methods, i.e., without the constraint of a prescribed motion duration. The main characteristics of these trajectories are listed in Tables 3 and 4, which are referred to motion laws applied, respectively, to the large and medium container. Since the optimization methods introduce a delay, the fourth column in both Tables indicates the trajectory total execution time. Like in Section 6.1, input shaping and IIR filters are applied to motion laws of $1s$ for the large vessel and $0.8s$ for the medium one; a chain of FIR filters is used to obtain an exact trapezoid acceleration trajectory satisfying the condition 14. Tables 3 and 4 report also data about motion laws with a duration of $1.4s$ for the large container (Traj. 3 and Traj. 4) and $1s$ for the medium container (Traj. 7). In this way, one can assess the effectiveness of the optimization techniques not only with respect to the original trajectories (Traj. 1, 2, 5), which have a shorter duration, but also with respect to non-optimized trajectories with a comparable or longer duration. In Tables 3 and 4 only the column $\Delta\overline{\eta}_{rest}$ is reported since the maximum sloshing height during the motion is strongly influenced by the movement duration, which is now different for different motion laws. The column $\Delta\overline{\eta}_{rest}$ reports two numbers: the first one is the reduction of the sloshing-height peak with respect to the short non-optimized trajectory ($1s$ for the large container and $0.8s$ for the medium one), while the second value is computed with reference to the long non-optimized trajectory ($1.4s$ for the large container and $1s$ for the medium one). The results show optimal damping of the free-surface vibration even for highly dynamic motions, with peak accelerations much higher (roughly $10m/s^2$) than those studied in the previous literature (approximately $2.5m/s^2$).

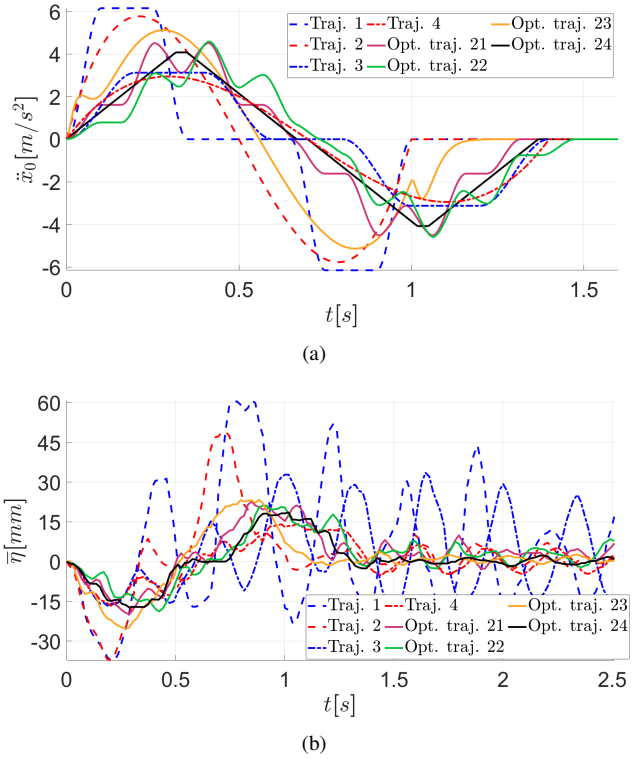

Fig. 12: Acceleration profiles (a) and system responses (b) with delay introduction (large container).

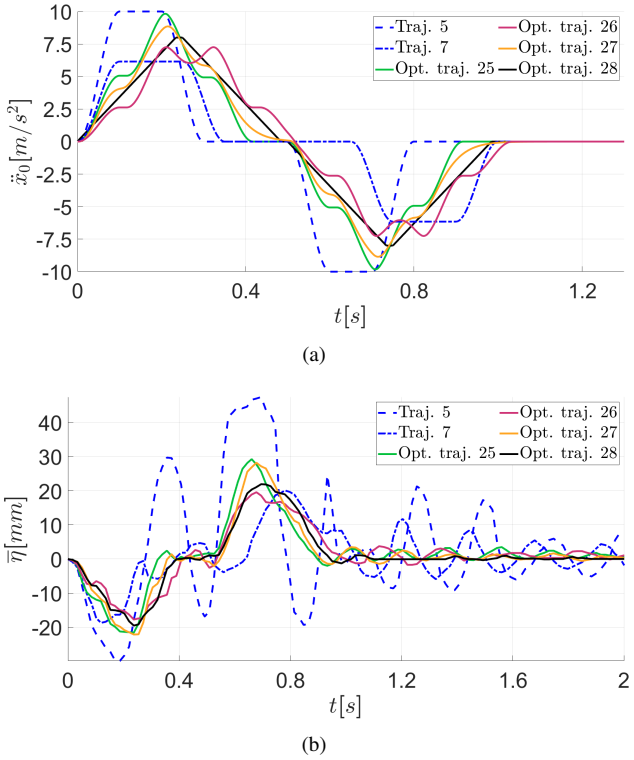

Fig. 13: Acceleration profiles (a) and system responses (b) with delay introduction (medium container).

7 Conclusions

Different methods to design anti-sloshing trajectories with a prescribed motion time were analyzed by applying them to highly-dynamical container trajectories, i.e., motion laws with maximum accelerations between $4m/s^2$ and $13m/s^2$. These methods are supposed to be particularly useful in automatic packaging machines, where the motion time is usually assigned and cannot be changed, and very fast movements are required to meet productivity demands. The objective of these trajectories is to reduce the stirring of the liquid both during the container motion and after its end.

Table 3: Comparison of the results obtained on the large container with different optimization methods applied with no prescribed motion duration (i.e., with the introduction of a delay).

Traj.	Original traj.	Opt. method	t_f $[s]$	$max(\ddot{x}_0)$ $[m/s^2]$	$max(\dot{x}_0)$ $[m/s]$	$max(\overline{\eta})$ $[mm]$	$max(\overline{\eta}_{rest})$ $[mm]$	$\Delta\overline{\eta}_{rest}$
Traj. 1	Mod. trap.	/	1.0	6.2	1.5	60.9	51.8	/
Traj. 2	Poly5	/	1.0	5.8	1.9	48.9	10.3	/
Traj. 3	Mod. trap.	/	1.4	3.1	1.3	32.8	33.5	/
Traj. 4	Poly5	/	1.4	2.9	1.3	14.1	6.6	/
Opt. traj. 21	Mod. trap.	IS-EI	1.32	4.5	1.5	22.7	10.0	$-80.7\%/-70.1\%$
Opt. traj. 22	Mod. trap.	IS-ZVDD	1.48	4.6	1.5	21.2	8.5	$-83.6\%/-74.6\%$
Opt. traj. 23	Poly5	IIR ($\tau = 50$)	1.19	5.1	1.8	23.4	3.8	$-63.1\%/-42.4\%$
Opt. traj. 24	/	FIR	1.37	4.1	1.4	18.6	2.3	$-95.6\%/-93.1\%$

Table 4: Comparison of the results obtained on the medium container with different optimization methods applied with no prescribed motion duration (i.e., with the introduction of a delay).

Traj.	Original traj.	Opt. method	t_f $[s]$	$max(\ddot{x}_0)$ $[m/s^2]$	$max(\dot{x}_0)$ $[m/s]$	$max(\overline{\eta})$ $[mm]$	$max(\overline{\eta}_{rest})$ $[mm]$	$\Delta\overline{\eta}_{rest}$
Traj. 5	Mod. trap.	/	0.8	10.0	2.0	47.5	24.6	/
Traj. 7	Mod. trap.	/	1.0	6.2	1.5	20.1	11.7	/
Opt. traj. 25	Mod. trap.	IS-ZV	0.92	9.8	2.0	29.3	3.5	$-85.7\%/-70.1\%$
Opt. traj. 26	Mod. trap.	IS-EI	1.03	7.3	2.0	19.6	3.8	$-84.6\%/-67.5\%$
Opt. traj. 27	Mod. trap.	IIR ($\tau = 40$)	1.04	8.9	2.0	28.2	3.5	$-85.7\%/-70.1\%$
Opt. traj. 28	/	FIR	0.98	8.0	2.0	21.9	1.3	$-94.7\%/-88.9\%$

In particular, four optimization methods were investigated, based on input shaping, dynamic-model inversion, IIR filters, and FIR filters. The inversion of the dynamic model was shown to be unsuitable and was discarded, whereas the other methods were experimentally compared. These methods were analyzed with the objective of application in real-time, namely generating motion laws that electric drives can directly calculate.

Experimental results proved the effectiveness of all methods based on FIR and IIR filters to build anti-sloshing motion laws, even in the case of highly dynamic motions. We notice that no optimization method seems a priori emerge above the others. In general, and according to physical intuition, the best technique is the one that guarantees the movement execution with the lowest maximum acceleration. The combination of the aforementioned anti-sloshing techniques and the sloshing prediction model described in [20] represents a complete instrument for the design of anti-sloshing motion laws, since, as a matter of fact, the designer can choose between different optimization methods by simulating the system response through the model shown in [20].

If one may not simulate the liquid sloshing caused by different trajectories, the recommended methods are input shaping and multi-segment trajectories built with 3 FIR filters. The first one applied to a polynomial trajectory is particularly suggested when the main objective is to minimize the maximum sloshing height during the container motion. In particular, since we are considering a prescribed motion duration, it is better to use a ZV shaper, which in general guarantees lower accelerations than more robust shapers. A multi-segment trajectory built with 3 FIR filters generally allows one to have the lowest residual vibration of the free surface and so it is recommended when the main objective is to minimize the oscillation in the rest phase. Both strategies are applicable in real-time and they do not require complex computations even for a prescribed duration of the motion. Finally, input shaping may be the preferred technique to be used in general: it is very simple and applies to any existing transport system, independently from the sampling period T_s, while the FIR-filter formulation in Eq. (15) cannot be applied

with good results when $T_s > 1ms$.

The effectiveness of the analyzed methods drops for accelerations higher than approximately $10m/s^2$.

Acknowledgment

This work was supported by Marchesini Group S.p.A., a leading company in the field of automatic packaging machines, especially for pharmaceutical and cosmetic products.

References

[1] H. Richter, 2010, "Motion Control of a Container With Slosh: Constrained Sliding Mode Approach," ASME, Journal of Dynamic Systems, Measurement, and Control, **132**(3), p. 031002.

[2] M. Grundelius and B. Bernhardsson, 1999, "Control of Liquid Slosh in and Industrial Packaging Machine," Proceedings of the 1999 IEEE International Conference on Control Applications, Kohala Coast, HI, USA, **2**, pp. 1654-1659.

[3] M. Grundelius, 2000, "Iterative Optimal Control of Liquid Slosh in an Industrial Packaging Machine," Proceedings of the 39th IEEE Conference on Decision and Control, Sydney, NSW, **4**, pp. 3427-3432.

[4] R. Di Leva, M. Carricato, H. Gattringer, and A. Müller, 2021, "Time-optimal trajectory planning for anti-sloshing 2-dimensional motions of an industrial robot," 20th International Conference on Advanced Robotics (ICAR 2021), Ljubljana, Slovenia, pp. 32-37.

[5] K. Yano and K. Terashima, 2005, "Sloshing suppression control of liquid transfer systems considering a 3-D transfer path," IEEE/ASME Transactions on Mechatronics, **10**(1), pp. 8-16.

[6] Y. Noda, K. Yano, S. Horihata and K. Terashima, 2004, "Sloshing Suppression Control During Liquid Container Transfer Involving Dynamic Tilting using Wigner Distribution Analysis," 2004 43rd IEEE Conference on Decision and Control (CDC), Nassau, **3**, pp. 3045-3052.

[7] J. Reinhold, M. Amersdorfer and T. Meurer, 2019, "A Dynamic Optimization Approach for Sloshing Free Transport of Liquid Filled Containers using an Industrial Robot," 2019 IEEE/RSJ International Conference on Intelligent Robots and Systems (IROS), Macau, China, pp. 2336-2341.

[8] W. Aribowo, T. Yamashita, K. Terashima and H. Kitagawa, 2010, "Input Shaping Control to Suppress Sloshing on Liquid Container Transfer Using Multi-Joint Robot Arm," 2010 IEEE/RSJ International Conference on Intelligent Robots and Systems, Taipei, pp. 3489-3494.

[9] W. Aribowo, T. Yamashita and K. Terashima, 2015, "Integrated Trajectory Planning and Sloshing Suppression for Three-Dimensional Motion of Liquid Container Transfer Robot Arm," Journal of Robotics, **2015**, pp. 1-15.

[10] B. Pridgen, K. Bai, and W. Singhose, 2010, "Slosh Suppression by Robust Input Shaping," 49th IEEE Conference on Decision and Control (CDC), Atlanta, GA, pp. 2316-2321.

[11] Q. Zang, J. Huang, and Z. Liang, 2015, "Slosh Suppression for Infinite Modes in a Moving Liquid Container," IEEE/ASME Transactions on Mechatronics, **20**(1), pp. 217-225.

[12] H. Peter and P. Thomas, 2010, "Slosh-Free Positioning of Containers with Liquids and Flexible Conveyor Belt," Journal of Electrical Engineering, **61**(2), pp. 65-74.

[13] A. AlSaibie and W. Singhose, 2013, "Experimental testing of liquid slosh suppression in a suspended container with compound-pendulum dynamics," 2013 9th Asian Control Conference (ASCC), Istanbul, pp. 1-6.

[14] A. Alshaya and K. Alghanim, 2020, "Command Shaping for Sloshing Suppression of a Suspended Liquid Container," ASME, Journal of Dynamic Systems, Measurement, and Control, **142**(12), p. 121003, doi: 10.1115/1.4047957.

[15] E. Khorshid and A. Al-Fadhli, 2020, "Optimal Command Shaping Design for a Liquid Slosh Suppression in Overhead Crane Systems," ASME, Journal of Dynamic Systems, Measurement, and Control, **143**(2), p. 021005, doi: 10.1115/1.4048357.

[16] A. Alshaya and D. Almujarrab, 2021, "A smooth polynomial shaped command for sloshing suppression of a suspended liquid container," Transactions of the Institute of Measurement and Control, **43**(2), pp. 278-294, doi: 10.1177/0142331220949304.

[17] Huang, Jie, and Zhao, Xinsheng, 2018, "Control of Three-Dimensional Nonlinear Slosh in Moving Rectangular Containers," ASME, Journal of Dynamic Systems, Measurement, and Control, **140**(8),p. 081016, doi: 10.1115/1.4039278.

[18] C. Melchiorri, L. Biagiotti, L. Moriello, A. Paoli, 2018, "Manipulating liquids with robots: A sloshing-free solution," Control Engineering Practice, **78**, pp. 129-141.

[19] J. Feddema, C. Dohrmann, G. Parker, R. Robinett, V. Romero, and D. Schmitt, 1997, "Control for slosh-free motion of an open container," IEEE Control Systems Magazine, **17**(1), pp. 29-36.

[20] L. Guagliumi, A. Berti, E. Monti and M. Carricato, 2021, "A Simple Model-Based Method for Sloshing Estimation in Liquid Transfer in Automatic Machines," in IEEE Access, **9**, pp. 129347-129357, doi: 10.1109/ACCESS.2021.3113956.

[21] R. Di Leva, M. Carricato, H. Gattringer, and A. Müller, 2021, "Sloshing dynamics estimation for liquid-filled containers under 2-dimensional excitation," 10th ECCOMAS Thematic Conference on Multibody Dynamics, Budapest, Hungary, pp. 80-89.

[22] R. A. Ibrahim, 2005, "Liquid Sloshing Dynamics: Theory and Applications," Cambridge University Press.

[23] H. F. Bauer, 1964, "Tables of Zeros of Cross Product Bessel Functions $J'_p(\xi)Y'_p(k\xi) - J'_p(k\xi)Y'_p(\xi) = 0$," Mathematics of Computation, **18**(85), pp. 128-135.

[24] L. Biagiotti, C. Melchiorri, 2008, "Trajectory Planning for Automatic Machines and Robots," Springer.

[25] N. C. Singer, and W. P. Seering, 1990, "Preshaping

Command Inputs to Reduce System Vibration," ASME, Journal of Dynamic Systems, Measurement, and Control, **112**(1), pp. 76–82.

[26] W. Singhose, W. Seering, and N. Singer, 1994, "Residual Vibration Reduction Using Vector Diagrams to Generate Shaped Inputs," ASME, Journal of Mechanical Design, **116**(2), pp. 654–659.

[27] R. Robinett, C. Dohrmann, G. Eisler, J. Feddema, G. Parker, D. Wilson, and D. Stokes, 2002, "Flexible Robot Dynamics and Controls," Springer.

[28] G. F. Franklin, J. D. Powell, M. Workman, 1998, "Digital Control of Dynamic Systems," Addison-Wesley.

[29] L. Biagiotti, C. Melchiorri, 2012, "Fir filters for online trajectory planning with time - and frequency - domain specifications," Control Engineering Practice, **20**(12), pp. 1385 – 1399.

[30] L. Biagiotti, C. Melchiorri, L. Moriello, 2016, "Optimal trajectories for vibration reduction based on exponential filters," IEEE Transactions on Control Systems Technology, **24**(2), pp. 609 – 622.

[31] P. Boscariol, D. Richiedei, 2017, "Robust point-to-point trajectory planning for non-linear underactuated systems: Theory and experimental assessment," Robotics and Computer-Integrated Manufacturing, **50**.

[32] B. Pridgen, B., K. Bai and W. Singhose, 2013, "Shaping Container Motion for Multi-Mode and Robust Slosh Suppression," AIAA J. of Spacecraft and Rockets, **50**(2), pp. 440-448.